Supplemental Information for

Compositional effect of two-dimensional AuPd bimetallic nanoparticle arrays fabricated with block copolymer techniques on catalytic activity of CO oxidation

Sun Mi Kim,[‡a,b] Jeong Ho Mun,[‡d] Si Woo Lee,[‡a,b] Hyesung An,[‡c] Hyn You Kim,*[c] Sang Ouk Kim,*[d] and Jeong Young Park *[a,b]

[a]*Center for Nanomaterials and Chemical Reactions, Institute for Basic Science, Daejeon 305-701, Republic of Korea*

[b]*Graduate School of EEWS and Department of Chemistry, KAIST, Daejeon 305-701, Republic of Korea*

[c]*Department of Materials Science and Engineering, Chungnam National University, Daejeon 34134, Republic of Korea*

[d]*Department of Materials Science and Engineering, KAIST, Daejeon 305-701, Republic of Korea*

†Authors contributed equally to this work.

*To whom the correspondence should be addressed. E-mail: jeongypark@kaist.ac.kr, sangouk@kaist.ac.kr, kimhy@cnu.ac.kr

Experimental information

Fabrication of oxide thin films and AuPd bimetallic nanoparticles on oxides

Synthesis of undoped and F-doped TiO_2 and CeO_2 thin films The undoped and F-doped titanium dioxide (TiO_2) and CeO_2 sols used in preparation of the oxide thin films were synthesized via the sol-gel process. The undoped TiO_2 was prepared using titanium tetrabutyloxide (TTBO) as the Ti precursor, diethanolamine (DEA) as the stabilizer, and ethyl alcohol (EtOH) as the solvent. All the reagents were analytical grade and used without further purification. The molar chemical composition of the starting solution was TTBO:H_2O:DEA:EtOH = 1:26.5:1:1. The solution was continuously stirred for 2 h for the formation of a transparent TiO_2 sol and aged for 24 h for fabrication of the thin films. The F-doped TiO_2 sol was synthesized using a procedure similar to that described above with the exception of adding ammonium fluoride (NH_4F) at a molar ratio of 0.1 as the fluorine precursor.[1] To create a thin film from the sols, silica wafers—ultrasonically cleaned with ethanol and water for 10 min and dried in nitrogen—were utilized as the substrate and the films were prepared on the SiO_2 wafer using the spin coating technique at 3000 rpm for 20 s. The fabricated thin films were preheated at 323 K for 1 h in an air-conditioned oven and annealed for 2 h at 623 K in a furnace to attain the anatase phase, which is considered the phase with the highest catalytic activity.

To prepare the CeO_2 thin film, the following materials were used: cerium chloride heptahydrate ($CeCl_3 \cdot 7H_2O$, Sigma-Aldrich), nitric acid (HNO_3, Daejung chemicals), myristyltrimethylammonium bromide ($CH_3(CH_2)_{13}N(Br)(CH_3)_3$, Sigma-Aldrich), and ethanol (C_2H_5OH, Merck chemicals). Cerium chloride heptahydrate and ethanol were used as the precursor and solvent, respectively.[2] Nitric acid helped the cerium chloride heptahydrate sols to form a gel and myristyltrimethylammonium bromide was used as a surfactant to make a uniform thin film. 0.252 g of cerium chloride heptahydrate and 0.126 g of myristyltrimethylammonium bromide were added to 20 ml of ethanol, and then mixed with 168 μl of nitric acid. The solution was mixed using a stirrer. The substrate on the spin coater was rotated at 3000 rpm for 30 s and was repeated 6 times to obtain a uniform thickness. After making the CeO_2 thin film, the film was preheated at 323 K for 1 h in an air-conditioned oven. The CeO_2 thin film was then annealed at 723 K for

1 h in a furnace.

Fabrication of AuPd bimetallic nanoparticles on oxides Fig. 1 shows the patterned single-crystalline AuPd nanoalloying array procedure and corresponding SEM images obtained using a Hitachi S-4800 FE-SEM. First, the thin films were prepared via self-assembly of asymmetric polystyrene-*block*-4-vinylpyridine (PS-*b*-P4VP) block copolymers (M_w: 24000 g/mol for the polystyrene (PS) and 9500 g/mol for the 4-vinylpyridine (P4VP) blocks, purchased from Polymer Source Inc.; dispersity index is 1.10). The thin film was spin casted from 0.5 wt% solutions in toluene/tetrahydrofuran (THF) = 3/1 (weight ratio) at 2400 rpm onto undoped and F-doped TiO_2 or CeO_2 substrates prepared using the sol-gel process. The perpendicular orientation of the cylindrical P4VP blocks was obtained on the substrate after a solvent annealing process under toluene/THF mixture vapor atmosphere for 6 h at room temperature. Solvent annealing of the PS-*b*-P4VP thin film with a cylindrical volume fraction results in the formation of a P4VP hexagonal cylinder in a PS matrix. Afterwards, chloroaurate ($AuCl^{4-}$) and chloropallate ($PdCl_4^{2-}$) anions, as a function of the concentration of the two metal precursors, were simultaneously loaded onto the perpendicularly oriented cylindrical P4VP blocks by immersing the samples into an aqueous HCl solution for 2 minutes. The pyridine group in the P4VP block is protonated in the HCl solution by the protons being attached to the nitrogen. Thus, when PS-*b*-P4VP is immersed in a solution containing a metal anion, the metal anion is adsorbed to the pyridine group in P4VP by an electrostatic interaction. Therefore, the $AuCl_4^-$ and $PdCl_4^{2-}$ ions dissolved in the solution are simultaneously adsorbed to the P4VP block and form a bimetallic nanocluster. After precursor loading, the sample was recovered and thoroughly rinsed with deionized water to remove any excess metallic anions (Fig. 1a). Finally, oxygen plasma treatment (7×10^{-2} Torr O_2, 50 W radio frequency power) of the entire sample was performed to completely remove the polymeric thin film and obtain AuPd nanocluster arrays (Fig. 1b). During the oxygen plasma process, non-metallic components, including PS, P4VP, and Cl, are removed. Thus, only the slightly oxidized AuPd nanocluster remains in a hexagonal position where the P4VP was present. Subsequent thermal treatment (reduction) under Ar/H_2 at 723 K for 1 h was performed for agglomeration of the nanoclusters and conversion into single-crystalline AuPd nanoalloy arrays (Fig. 1c). During thermal treatment, the oxidized

nanoclusters were reduced to metallic AuPd and the structural composition was maintained as a core-shell model. Furthermore, the core-shell structure was formed during thermal treatment as a result of agglomeration and relocation of the Au and Pd atoms. Fig. S1 shows size distribution histograms of the AuPd nanocatalysts formed as a function of the concentration of the Au and Pd precursors. Fig. S2 shows size distribution histograms of the AuPd nanocatalysts synthesized with different concentrations of the Au and Pd precursors and reaction times, indicating the ability to tune the size of the nanocatalysts.

Characterization of the AuPd bimetallic nanoparticles on oxides

Morphology and composition of the AuPd bimetallic nanoparticle arrays The morphologies of the block copolymer thin films and AuPd nanoalloy arrays were observed using a Hitachi S-4800 FE-SEM (Fig. 1d–f). A Cs-corrected JEM-ARM200F HR-TEM was used for crystalline structure imaging and chemical composition analysis of the nanoalloy arrays formed as a function of the concentration of the two metal precursors (Fig. 2b). During preparation of the sample for TEM characterization, the back of the substrate was polished out, followed by carbon deposition for sample protection. The AuPd nanoalloy arrays remaining on the thinner substrate were transferred to copper grids (GA2000-Cu, 2 mm aperture). Subsequent ion milling was done until the sample thickness was 2–3 μm. The EDS measurement data were acquired from the Au-L and Pd-K edges and the chemical composition of the nanoalloys is the averaged value from seven nanoalloys creating a hexagonal array. The XPS spectra, a technique more sensitive to the surface, were taken using a Thermo VG Scientific Sigma Probe system equipped with an Al-Kα X-ray source (1486.3 eV) and energy resolution of 0.47 eV FWHM to analyze the surface chemical composition of the nanoalloying catalysts.

Catalytic reaction

CO oxidation on the AuPd bimetallic nanoalloys on oxides The CO oxidation reaction was carried out under 40 Torr CO and 100 Torr O_2 as the reactant gases and 620 Torr He as the balancing gas in a batch reactor equipped with a recirculation pump. The gases were circulated through the reaction line by a Metal Bellows recirculation pump. A gas chromatograph equipped with a thermal conductivity detector and

6′×1/8″ SS molecular sieve 5A was used to separate the products for analysis. The measured reaction rates are reported as turnover frequencies (TOF) and are measured in units of product molecules of CO_2 produced per metal surface site per second of reaction time. Because the reaction process is relatively slow and the reaction was carried out in the low-conversion regime (less than 10%), we assume that the reaction data were obtained in a kinetically-controlled regime. The number of metal sites is calculated using the geometry based on SEM measurements of the surface area of the nanoparticle arrays.

Density functional theory calculations

To estimate the energetics of Pd surface segregation under CO oxidation conditions, we calculated the driving force, ΔE, of the Pd surface segregation driven by CO and O_2. For example, the ΔE of CO-driven Pd surface segregation was calculated by comparing the total energy of the AuPd alloy + CO system with two different Pd locations: sub-surface or surface. We used a 4×4×4 Au(100) slab model as a reference structure for the AuPd alloy. A single Pd atom was located at either the sub-surface or surface layer and each model was optimized. The bottom two layers were fixed upon optimization. The binding energies, E_{bind}, of the CO, O_2, and H_2 molecules on the AuPd alloy models were calculated by locating the adsorbing molecules at the closest position to the Pd atom.

We performed spin-polarized density functional theory (DFT) calculations with the Vienna ab-initio simulation package (VASP).[3] The exchange-correlation energy of the Kohn–Sham equation was functionalized with the Perdew, Burke, and Ernzerhof functional[4] and the interaction between the valence electrons and the ionic core was described by the projector augmented wave method.[5] Valence electron functions were extended with the plane-wave basis to an energy cutoff of 400 eV. A 2×2×1 grid was applied to sample the Brillouin zone. The convergence criteria for the electronic structure and the geometry were set to 10^{-4} eV and 0.01 eV/A, respectively. We used a Gaussian smearing function with a finite temperature width of 0.2 eV to improve the convergence of states near the Fermi level.

Construction of ΔG diagrams of CO or O_2 adsorption using DFT calculations

The ΔG of CO or O_2 adsorption on AuPd alloy surfaces (refer to Fig. 5 for the geometries) was calculated as follows:

$$\Delta G(CO) = E(CO + AuPd) - E(AuPd) - \{E(CO) + \Delta\mu_{CO}\}$$

$$\Delta G(O_2) = E(O_2 + AuPd) - E(AuPd) - \{E(O_2) + \Delta\mu_{O_2}\}$$

where *E*(system) is the DFT-estimated total energy of a corresponding system. The chemical potential of CO and $\Delta\mu_{CO}$, the chemical potential difference, are given by

$$\mu_{CO}(T,p) = \Delta H(0K, p^0 \rightarrow T, p^0) - T\Delta S(0K, p^0 \rightarrow T, p^0) + kT\ln\left({}^{p}/_{p^0}\right)$$

$$\Delta\mu_{CO} = \mu_{CO}(T,p) - E(CO)$$

where p^0 is set to 1.013 bar and $\mu_{CO}(0K, p^0) = E(CO)$. We used the same approach to estimate the chemical potential of O_2 and $\Delta\mu_{O_2}$. The tabulated temperature-dependent enthalpy and entropy values of CO and O_2 were adopted from the NIST chemistry web-book[6] and NIST-JANAF thermochemical tables.[7] We estimated the entropic contribution to the ΔG of CO adsorption using the experimentally verified Campbell's model.[8] The following linear relationship between the entropy of a gas-phase molecule and an adsorbed molecule was applied: $S^0_{adsorbed\ molecule} = 0.7\, S^0_{gas-phase\ molecule} - 3.3\, R$. The calculated ΔG values of CO or O_2 adsorption on the AuPd alloy surfaces with different Pd locations were plotted as a function of the $\Delta\mu$ of the gas-phase molecules (Fig. S6).

(a)

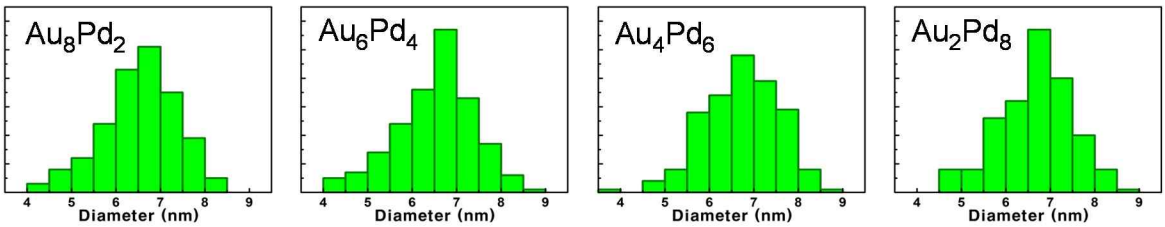

(b)

1 mM, 1 min	Au_8Pd_2	Au_6Pd_4	Au_4Pd_6	Au_2Pd_8
Ave. dia. (nm)	6.6	6.7	6.5	6.5
Std. dev. (nm)	0.80	0.83	0.87	0.84

Fig. S1. (a) Size distribution histograms and (b) summary table for the AuPd nanocatalysts formed as a function of the concentration of the Au and Pd precursors.

(a)

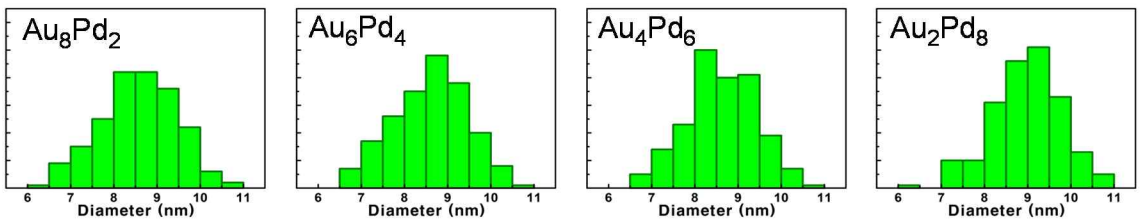

(b)

2 mM, 5 min	Au_8Pd_2	Au_6Pd_4	Au_4Pd_6	Au_2Pd_8
Ave. dia. (nm)	9.0	8.6	8.6	8.5
Std. dev. (nm)	0.81	0.89	0.84	0.88

Fig. S2. (a) Size distribution histograms of the AuPd nanocatalysts and (b) summary table where the synthesis used different concentrations of the Au and Pd precursors (2 mM) and an extended reaction time (5 minutes).

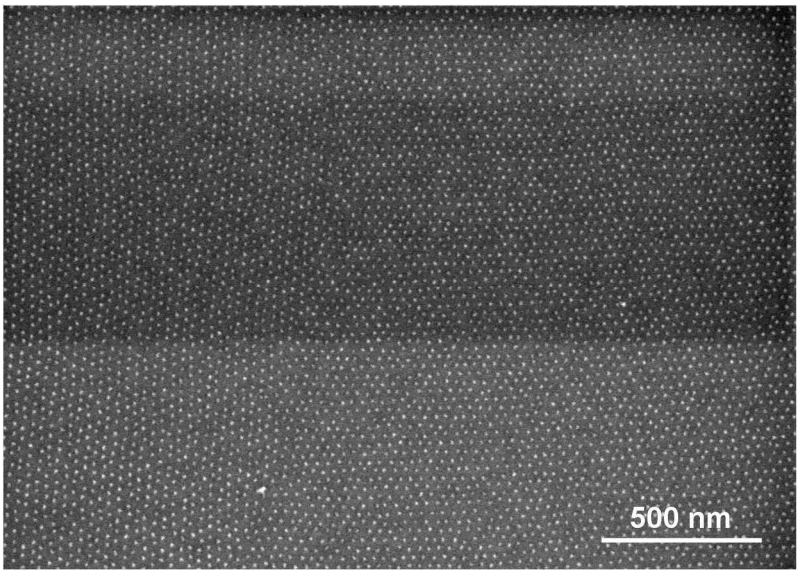

Fig. S3. Large-scale SEM image of the prepared AuPd nanoalloy array following the removal of the polymer and thermal treatment.

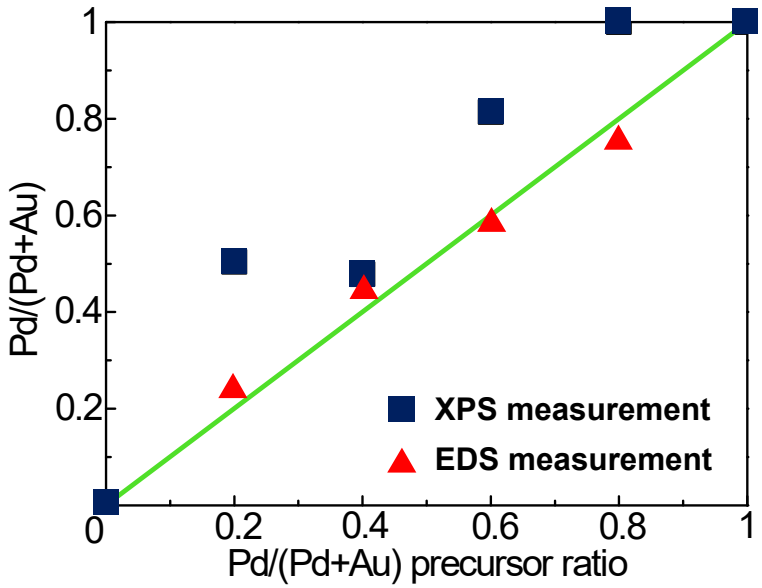

Fig. S4. Comparison of the Pd chemical composition determined by XPS measurement using the sensitivity factors for Pd and Au and the integrated peak areas of Pd3d, Au4f, and Pd chemical compositions determined by EDS measurement versus the Pd/(Pd+Au) precursor ratio.

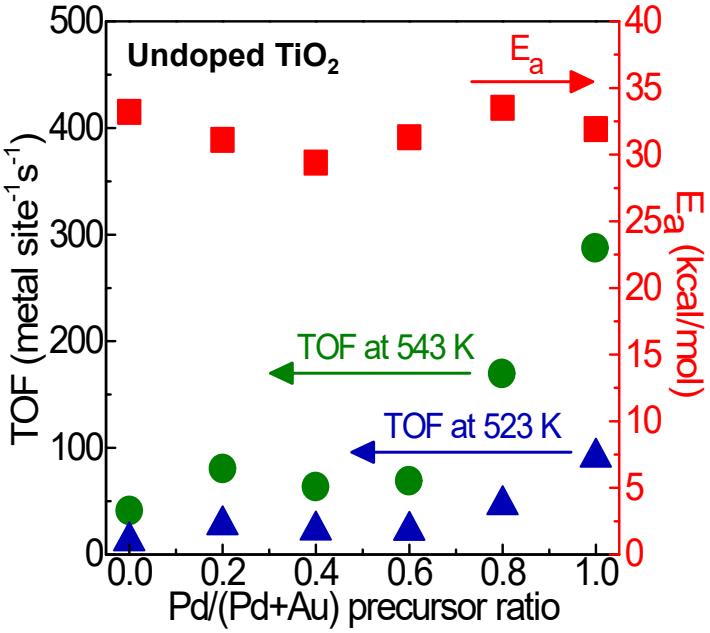

Fig. S5. Turnover rates at 523 and 573 K and activation energies measured on the Au_xPd_{10-x} nanoalloy catalysts supported on undoped TiO_2 substrate for the CO oxidation reaction as a function of the mole fraction of the Pd and Au metal precursors.

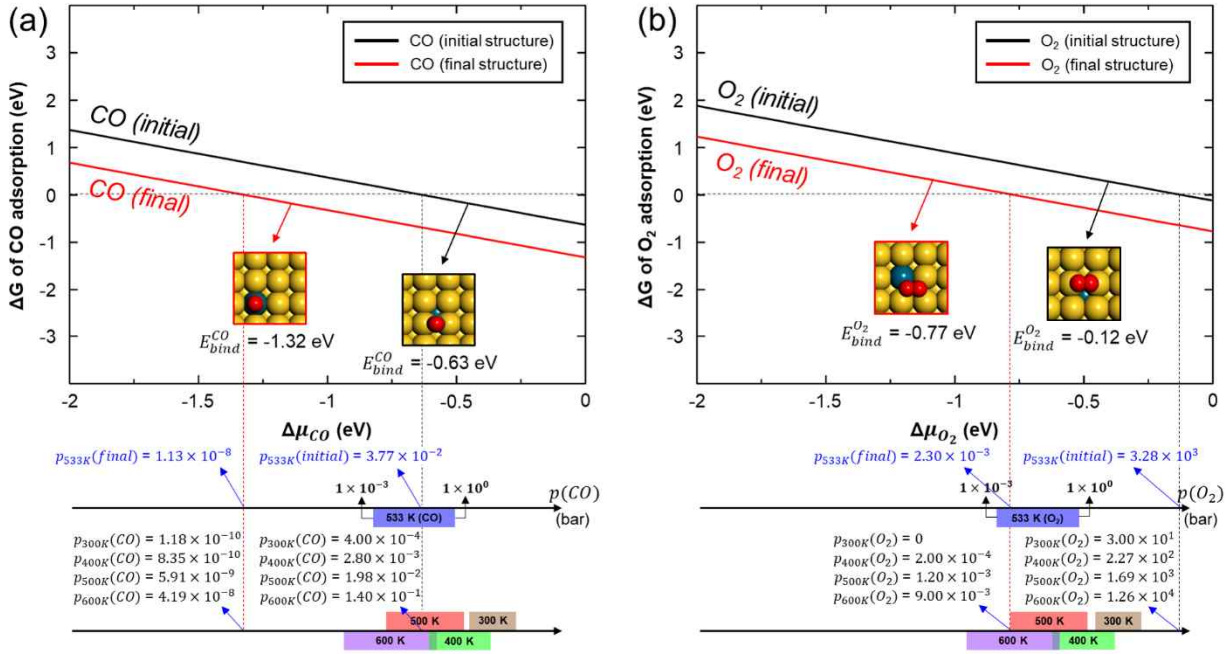

Fig. S6. ΔG diagrams of (a) CO and (b) O_2 adsorption presented as a function of the Δμ of CO or O_2. The solid red and black lines represent the ΔG of the initial and the final state geometries, respectively. The vertical dotted lines show the minimum Δμ for stabilization of the adsorbed molecules. The colored boxes below the diagrams present the p(CO) or $p(O_2)$ range (0.001 to 1.00) at the given temperatures. Because Δμ is a function of the temperature and partial pressure of the gas-phase molecule, p(CO) and $p(O_2)$ at several reference temperatures are presented. The points where the vertical dotted lines cross the colored boxes indicate the corresponding p(CO) or $p(O_2)$ at the reference temperatures.

References

1. K. C. Goddeti, S. M. Kim, Y. K. Lee, S. H. Kim and J. Y. Park, *Catal. Lett.*, 2014, **144**, 1411-1417.
2. D. Park, S. M. Kim, S. H. Kim, J. Y. Yun and J. Y. Park, *Appl. Catal., A*, 2014, **480**, 25-33.
3. G. Kresse and J. Furthmuller, *Phys. Rev. B*, 1996, **54**, 11169-11186.
4. J. P. Perdew, K. Burke and M. Ernzerhof, *Phys. Rev. Lett.*, 1996, **77**, 3865-3868.
5. P. E. Blochl, *Phys. Rev. B*, 1994, **50**, 17953-17979.
6. NIST Chemistry WebBook. http://webbook.nist.gov (accessed October 15, 2018)
7. M. W. Chase, *NIST-JANAF Thermochemical Tables*, 4th ed.; *Journal of Physical and Chemical Reference Data Monograph No.9*; American Institute of Physics: Woodbury, NY, 1998; pp 1-1951.
8. C. T. Campbell and J. R. V. Sellers, *Chem. Rev.*, 2013, **113**, 4106-4135.